INTERNATIONAL JOURNAL FOR NUMERICAL METHODS IN FLUIDS
Int. J. Numer. Meth. Fluids 2002; **39**:855–864 (DOI: 10.1002/fld.333)

Eddy resolving simulations of turbulent solar convection

Julian R. Elliott*,[1,†] and Piotr K. Smolarkiewicz[2]

[1]*Eurobios UK, 5 High Timber St., London, U.K.*
[2]*National Centre for Atmospheric Research, Boulder, CO, U.S.A.*

SUMMARY

Deep convection occurs in the outer one-third of the solar interior and transports energy generated by nuclear reactions to the surface. It leads to a characteristic pattern of time-averaged differential rotation, with the poles rotating significantly slower (approximately 25 per cent) than the equator. This differential rotation results from Reynolds stresses that are associated with correlations of the longitudinal velocity with the radial and latitudinal velocities. One particularly interesting feature of the solar differential rotation is that it shows significant tilting of angular velocity contours away from the rotation axis (i.e. breaking of the Taylor–Proudman state of rotation rate constant on cylinders aligned with the rotation axis), in contrast to the results from early numerical simulations. In spite of such discrepancies, numerical simulations provide the best chance of making progress in understanding the observations. Many studies have adopted the DNS approach and have justified the artificially large viscosities and thermal diffusivities used as modelling transport by unresolved eddies. LES techniques (which use a turbulence closure to relate transport coefficients to local properties of the flow) offer a superior alternative, but face the problem of defining the turbulence closure, which is potentially difficult in the presence of stratification, rotation and other complicating factors. This problem can be avoided by shifting the responsibility for truncating the turbulent cascade from an explicit turbulence closure to the numerical scheme itself. Since this approach abandons the rigorous notions of the LES approach, we refer to it as a VLES (Very Large Eddy Simulation). This paper compares results of DNS simulations carried out with a spherical-harmonic code, and preliminary results obtained using a VLES-type code. Both make the anelastic approximation. Copyright © 2002 John Wiley & Sons, Ltd.

KEY WORDS: convection; solar interior; differential rotation

1. INTRODUCTION

In the outer one-third of the solar interior, radiative transport becomes inefficient at transporting energy outwards (due to the increasing opacity) and convection takes over as the primary mechanism of energy transport; this region of the sun is known as the *convection zone*. The convection is driven primarily by strong radiative cooling near the surface, with compensating warming occurring over a broad region in radius near the base of the convection zone. The time scale of the convection is about 30 earth days, with characteristic velocities of a few

* Correspondence to: J.R. Elliott, Eurobios UK, Sir John Lyon House, 5 High Timber Street, London EC4V 3NX, UK.
† E-mail: julian.elliott@eurobios.com

Received October 2001
Revised December 2001

hundred metres per second and characteristic temperature fluctuations of a few Kelvin. Since the convective time scale is very similar to the rotation time scale (giving a Rossby number of order 1), the convection is significantly influenced by rotation, leading to the observed differential rotation with the poles rotating substantially slower than the equator (see Plate 1). In addition, because the density in the convection zone varies by over 10 orders of magnitude, the convection is strongly influenced by stratification effects. Since solar plasma is a very good electrical conductor (leading to small magnetic diffusivities and high magnetic Reynolds numbers), magnetic fields are yet another factor which influences the dynamics of the solar interior; the interaction of fluid flow and magnetic fields leads to the 22 year cycle of magnetic fields and sunspot activity, although the exact mechanism is as yet unclear.

The combined effect of compressibility, rotation and magnetic fields in a high Reynolds number (and therefore highly turbulent) flow leads to system with a rich spectrum of behaviour that we can only hope to understand through detailed numerical simulations. Such numerical simulations, which are computationally intensive, have only become possible in the last few decades with the advent of high performance computing. In spite of the advances in computer performance, the large number of degrees of freedom necessitates adopting certain approximations in carrying out simulations of solar convection—the most important of these is to adopt the *anelastic* approximation (see Reference [2]). This filters out fast sound waves that would otherwise unreasonably limit the computational time step, and which probably play a small part in the overall dynamics of the convection zone. Both simulations described in this paper make this approximation. Another fundamental simplification is to neglect magnetic fields; this is probably a reasonably good approximation if magnetic fields in the convection zone are not too strong. A final simplification made in the simulations described in this paper is to limit the range of densities modelled, effectively cutting the simulation off near the solar surface where the density scale height becomes small; this removes the need to use multiple grids to model the different scales of convection and simplifies the problem.

A question that is paramount in modelling solar convection is which numerical integration scheme to adopt. Interestingly, the thermodynamic properties of convection provide some insight in answering this question. Radiative heating near the base and cooling near the surface act as a source of negative entropy, which in equilibrium must be compensated for by the action of irreversible processes. Two irreversible processes contribute—firstly, the transfer of heat from one fluid element to another by radiative diffusion, and secondly, the dissipation of kinetic energy by the action of viscosity. The relative roles of the two are unclear, although since the Prandtl number is low (the radiative diffusivity being much higher than the kinematic viscosity) the first is probably dominant. Unfortunately, since the radiative diffusivity and kinematic viscosity are both so small in the solar convection zone, the scales at which they operate are far too small to be resolved computationally. For this reason, irreversible entropy production must be accounted for by artificial dissipation, either in the form of enhanced values of the radiative diffusivity and viscosity, or a dissipative numerical scheme. Simulations that employ non-dissipative advection schemes, which include pseudo-spectral and CTS (Centred in Time and Space) methods, thus have no chance of producing stable solutions unless explicit thermal diffusion and viscosity are added. Such methods were used in the many early simulations of solar convection, the necessary diffusion and viscosity being justified as in some way modelling the effect of small eddies on the large-scale flow (e.g. References [3, 4]). Since the diffusion and viscosity took the form of Laplacians with constant coefficients, these studies may be classified as DNS simulations. The

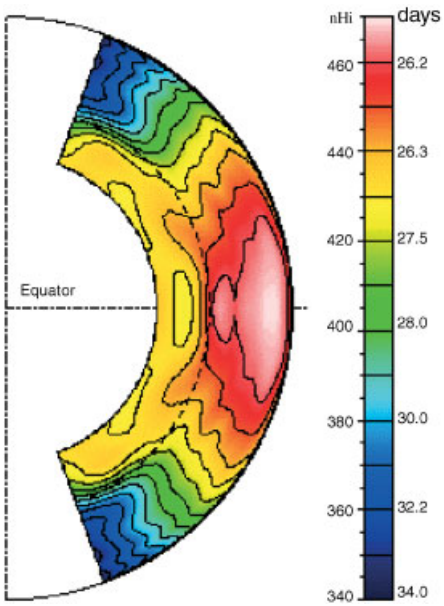

Plate 1. Solar angular velocity in a meridional cut as determined by helioseismic inversion of GONG (Global Oscillations Network Group) data [1]. Note that polar rotation rate estimates are extrapolated from lower latitudes.

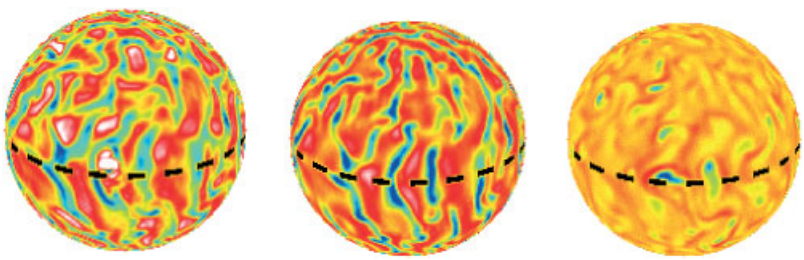

Plate 2. The vertical velocity on three horizontal surfaces (near the top, near the middle, and near the bottom) in a DNS simulation of solar convection. Red and white denote upflows, while blue denotes downflows.

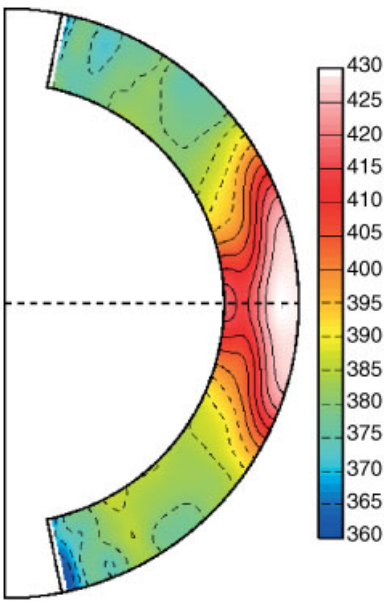

Plate 3. The time-averaged angular velocity from the same simulation as shown in Plate 2. The scale on the right is in nHz.

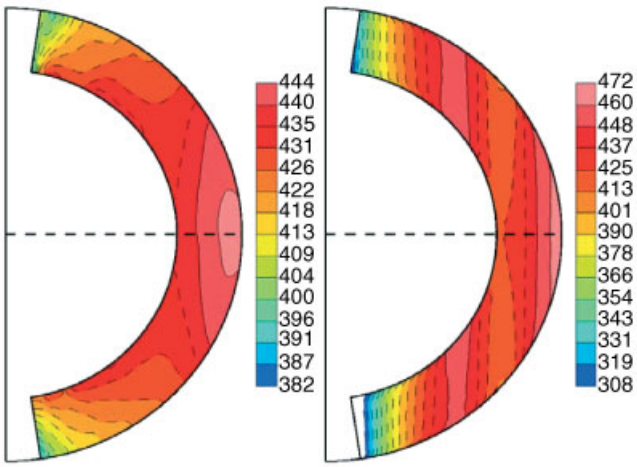

Plate 4. The time-averaged angular velocity in two simulations carried out using the NFT code. The one on the left is a DNS simulation for comparison with Plate 3, while the one on the right is a genuine VLES simulation.

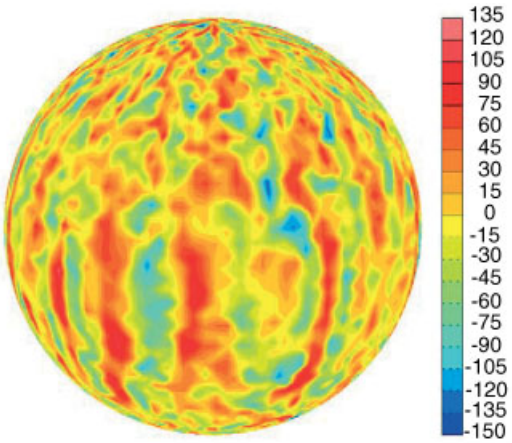

Plate 5. The vertical velocity on a horizontal surface near the middle of the domain for the VLES simulation. The scale on the right is in ms^{-1}.

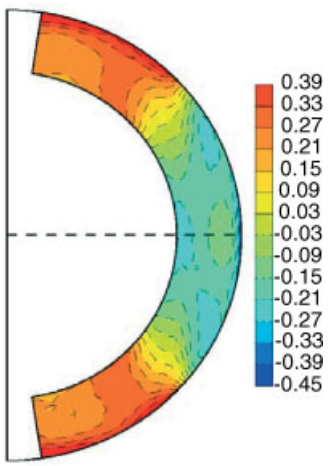

Plate 6. Longitudinally averaged potential temperature departures from the spherical mean in the VLES simulation.

next section summarizes some of the results from References [5] and [6], which fall into this category.

The problem with DNS techniques is that large thermal diffusivities and viscosities are introduced everywhere, even when the flow is laminar. A better approach is to adopt the LES technique, where the flow field is decomposed into resolved and unresolved scales, and filtered equations are obtained which include the divergence of the SGS (Sub-Grid Scale) stress tensor. In general, the components of this stress tensor are uncomputable and must be expressed in terms of the resolved components of the flow variables—this is known as an SGS model. The most commonly used SGS model is that postulated by Smagorinsky [7], in which the SGS stress tensor is proportional to the local rate of strain of the resolved flow.

Historically, SGS models have tended to be judged not so much on being sound representations of what is actually happening on the sub-grid scale as on effectively suppressing false computational oscillations. Once one gives up the notion that SGS models accurately represent the behaviour of unresolved eddies, there are simpler, more effective, means of achieving the suppression of false computational oscillations. In particular, there is a class of finite difference methods—non-oscillatory forward in time (NFT)—that have exhibited the remarkable property of representing LES/VLES without recourse to any explicit SGS model. Such methods are inherently dissipative and provide an irreversible entropy source, as they must do given the constraints mentioned above. They have demonstrated their utility in simulations of the Earth's planetary boundary layer (PBL) [8], comparing well with equivalent LES runs. This paper presents first results obtained for solar convection using a code based on NFT methods, in particular the MPDATA (Multidimensional Positive-Definite Advection and Transport Algorithm) scheme [9].

Comparisons *have* previously been made between different numerical techniques for simulating solar convection [10]. In this work three-dimensional Cartesian convection was studied with both a pseudo-spectral code and a code that implemented the PPM algorithm (Piecewise Parabolic Method, see Reference [11]); the latter is another method from the NFT class, which can be run stably with no explicit diffusion or viscosity. Detailed comparisons of results were not presented in this study, but a description of the philosophy of NFT methods was included. It seems a great deal of avoidable confusion has been introduced into the subject by the use of the word inviscid to describe simulations using NFT methods.

This paper is divided into three sections after this introduction. The next section describes results from a pseudo-spectral DNS model, using constant diffusivities and viscosities. Section 3 describes results from a VLES simulation of solar convection, while Section 4 highlights the conclusions from this work. Finally, an appendix describes the equation set used in both the models described in this paper.

2. DNS RESULTS

This section describes numerical simulations carried out within the DNS framework, using a code (see References [5, 6, 12]) that expands the prognostic variables (entropy, pressure, and velocity) in spherical harmonics in the horizontal, and in Chebyshev polynomials in the vertical. Spherical harmonic expansions have been used widely in meteorological applications, and have the advantage of providing uniform resolution over the sphere (at least when triangular truncation is used)—this avoids computational artifacts near the poles. Non-linear terms

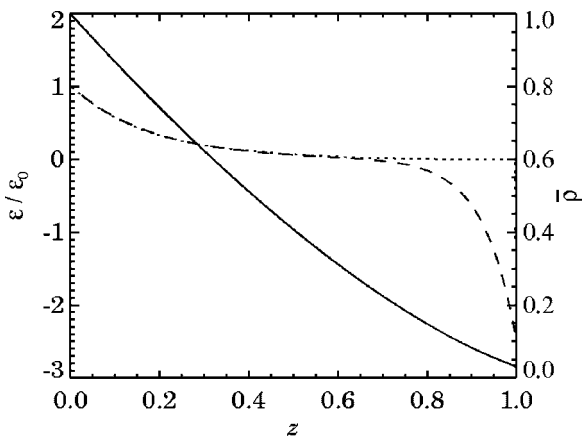

Figure 1. The divergence of the radiative flux (dotted line: actual, dashed line: that assumed in the model) and the variation of density with height (solid line), as functions of the fractional height z.

are calculated in physical space, using a grid with sufficient resolution to avoid quadratic aliasing. Apart from the uniform resolution, spherical harmonic basis functions also offer the advantage of yielding a very easy solution of the elliptic pressure equation, since the linear terms decouple.

The computational domain used for the simulations is a spherical shell with an inner radius of 5×10^5 km and an outer radius of 6.9×10^5 km. The density contrast from the bottom of the domain to the top is about 30, which, although substantially less than the actual contrast across the convection zone, allows for significant stratification effects to be felt. Thermal forcing is modelled by assuming that the mean stratification in the bulk of the convection zone is always nearly adiabatic, allowing the divergence of the radiative flux to be calculated fairly accurately (assuming a knowledge of the radiative opacity)—Figure 1 shows the divergence of the radiative flux as used in the simulations described here (for the exact formula used, see the appendix), along with the density (which is simply an adiabatic stratification). Near the surface the assumption of a near-adiabatic stratification breaks down, and there is an extremely narrow region of strong radiative cooling—this is artificially broadened (by making the scale of the region comparable to the local density scale height) to enable it to be resolved on the computational grid used.

Consistent with the DNS framework, the Navier–Stokes equations are solved with entropy diffusion and viscous terms having coefficients that depend only on radius. Tests have been carried out with several different dependencies of these coefficients on radius—the effects on the results are not too substantial. Sufficiently large values of entropy diffusion and viscosity are required to produce stable, well-behaved solutions; typical values used lead to Reynolds numbers in the region of ~ 50. In a linear analysis, the most unstable modes of the system are convective rolls aligned with the rotation axis. These are also seen in the non-linear solutions, albeit with considerable distortion from non-linear effects. Plate 2 shows a typical view of the vertical velocity on three levels in a solution from the DNS code. The convective rolls, or 'banana cells', can clearly be seen in the left and middle panels of this figure (which correspond to levels near the surface, and near the centre of the convection zone,

respectively), with rotationally aligned lanes of downflowing material aligned interspersed by upflowing material.

This simulation was carried out with spherical harmonics up to degree 85, and with 64 radial grid points. The Reynolds number for the largest eddies in this simulation was about 30. Simulations can be carried out with higher resolutions, enabling higher Reynolds numbers to be attained; however, the computational effort required to increase the resolution is very high, since the number of floating point operations scales with the fifth power of resolution (since the spherical harmonic transforms scale with the cube of the horizontal resolution, and the number of time steps also scales linearly with the resolution).

Turning now to other aspects of the results, the time-averaged differential rotation in the same simulation is shown in Plate 3. Comparing with Plate 1, which shows the solar differential rotation (as deduced from helioseismology), some similarities are clear. Firstly, the simulation gives a fast equator and slow poles, which is correct. Secondly, the contrast in angular velocity between the poles and equator is similar to that seen in the sun. Unfortunately, there are significant differences in other respects. Firstly, most of the angular velocity contrast in the simulation is seen near the equator, whereas Plate 1 shows that in the sun there is a continuous change in angular velocity from the equator to the poles. Also, Plate 1 shows significant tilting of lines of constant angular velocity relative to the rotation axis, whereas the simulation shows very little. Other simulations (see References [3] and [4]) have also shown little such tilting, with angular velocity contours nearly parallel to the rotation axis. The reasons for these discrepancies are currently unclear, although what does seem to be the case is that Reynolds stresses alone (in this case correlations of the radial and latitudinal velocity components) are not strong enough, and are typically of the wrong sign, to produce the observed tilting—buoyancy forces almost certainly play a part, implying that the poles are warm with respect to the equator.

The final aspect of the DNS results that we consider here is the mean meridional circulation. This circulation is driven by Reynolds stresses corresponding to correlations of the latitudinal and radial velocities and is important for dynamo wave propagation, especially near the base of the convection zone. The results (not shown) document pole-ward flows near the surface in both hemispheres (in agreement with results from helioseismology [13]) with equator-ward return flows deeper down. The magnitude of both of these flows is of the order of $10\,\mathrm{ms}^{-1}$.

3. LES RESULTS

The simulations described so far rely on comparatively large, fixed, values of viscosity and thermal diffusivity in order to obtain a stable solution. A better option is to use thermal diffusion and viscosities having coefficients that depend on local properties of the flow, such as the local rate of strain (which would be an LES approach). This avoids the use of a large amount of dissipation where it is unnecessary, the only drawback being the difficulty in finding general forms for these coefficients (especially in the presence of rotation and stratification). Another way of achieving the same objective, without this drawback, is to make the numerical advection scheme itself inherently stable. Such advection schemes belong to the general class of NFT methods for which ensuring linear stability (in particular by respecting the familiar Courant number condition) also assures nonlinear stability, at the expense of adding dissipation

in certain parts of the flow. We refer to numerical simulations of fluid flow employing such advection schemes as VLES, to distinguish them from LES simulations.

This section describes numerical simulations of solar convection carried out using a code described in Reference [14], and employing the VLES philosophy. It is an anelastic, grid-based code, with options for carrying out advection either by means of a semi-Lagrangian scheme or an Eulerian scheme (MPDATA, see Reference [9]). Because NFT methods are inherently two time-level, accurate time integration necessitates the solution of a large non-symmetric linear system that represents a complex non self-adjoint 3D elliptic PDE for pressure. For deep fluids, such as the sun's convection zone, such a problem can be solved using standard Krylov subspace methods (although note that in the case of the Earth's atmosphere, the resulting elliptic equations are extremely stiff, and preconditioning is necessary)—this is the approach adopted in this code.

Coordinate singularities, such as that present at the poles in the spherical polar coordinate system, represent a potential difficulty for grid-based methods. This is generally not particularly significant when simulating the Earth's atmosphere, since there is not much convective activity near the poles, but could present a problem in the solar case, since convection occurs at all latitudes with nearly equal strength.

Several simulations have been carried out using the code described in this section. Plate 4 shows the differential rotation obtained in two such simulations, of which the one on the left is a DNS-like simulation for comparison with the results of Section 2, while the one on the right is a genuine VLES simulation, with no added thermal diffusion or viscosity. The DNS-like simulation shown in the left-hand panel was carried out using similar values of viscosity and thermal diffusivity as those used in the simulation that yielded Plate 3. Comparing the two plots, it can be seen that the overall contrast in angular velocity between the equator and poles is similar, amounting to about 15 per cent of the equatorial value. This is somewhat less than the corresponding contrast seen in the sun (approximately 25 per cent). Looking beyond this simple measure, the new simulation is more 'solar-like' in two principal ways—first, quite a bit of the angular velocity contrast occurs near the poles, as opposed to having an almost constant angular velocity at latitudes above 30 degrees. Secondly, the contours of constant angular velocity are considerably tilted with respect the rotation axis, showing significant departure from the Taylor-Proudman regime.

The right-hand panel of Plate 4 shows the time-averaged angular velocity from the genuine VLES simulation, carried out using the Eulerian advection scheme. The angular velocity is seen to peak at the equator and at mid-latitudes, with weak minima at around 40 degrees latitude and strong minima near the poles. The overall contrast in angular velocity between the equator and poles is very large, larger indeed than in both the DNS simulation described in Section 2, and in the real sun. The contours of constant angular velocity are very nearly parallel to the rotation axis in this case, showing little breaking of the Taylor–Proudman state. This simulation clearly shows less similarity with the sun in differential rotation than either of the DNS simulations described—why should this be the case?

At this point it is worth considering a few of the possible reasons why the VLES simulation should give a less realistic differential rotation profile than either of the DNS simulations. The limitations of the VLES simulation can be broadly grouped into two categories—problems with the physics used, and insufficient resolution to capture the smallest eddies in the flow. Problems with the physics include insufficient density contrast between the bottom and top of the domain, inaccurate boundary conditions, and the absence of magnetic fields. Insufficient

resolution refers to the inability to model the smallest eddies in the flow as simulated, and would be manifested as a lack of good convergence with increasing numerical resolution. The DNS simulations share the same limitations, but suffer from the additional limitation of having excessive dissipation acting where it is not strictly necessary. It thus seems that although the DNS simulations are obtaining a better result, it is probably for the wrong reasons.

Turning now to other aspects of the solutions obtained with the NFT code, Plate 5 shows the vertical velocity from the VLES simulation on a horizontal surface at approximately the midpoint of the shell in radius. Close similarities can be seen with the vertical velocity from the spherical-harmonic code DNS simulation (shown in Plate 2), with elongated 'banana cells' near the equator, and less rotationally influenced convection near the poles. The maximum velocity of the downflows is somewhat higher than that of the upflows, while the absolute magnitudes are of the order of 100–150 ms^{-1}. The simulation shows some evidence of coordinate problems near the poles, with the typical scale of convective features diminishing in those regions—the danger of this occurring was noted in the introduction to this section.

Plate 6 shows the longitudinally averaged departures of the potential temperature from the spherical mean value in the VLES simulation. This plot shows how small the departures are, and how close the convection zone is to being spherically symmetric—the fluctuation in temperature is of the order of one part in a million. Efforts to measure the variation of the solar surface temperature and luminosity with latitude are thus faced with a very challenging problem. The small variation of temperature with latitude that this plot *does* show is such as to produce a thermal wind circulation that tends to tilt the lines of constant angular velocity away from the rotation axis; importantly, since the poles are warm with respect to the equator, this tilting is in the right direction (see the comment in the penultimate paragraph of Section 2). Note that little evidence of such tilting is actually seen in the angular velocity plots of Plate 4, presumably because the magnitude of the pole-equator temperature difference is not sufficiently large.

The mean meridional circulation generated in the VLES run (not shown) is found to be very similar to that obtained in the DNS case (see the last paragraph of Section 2) with a characteristic pole-ward flow near the surface and an equator-ward return flow deeper down. The magnitudes of these flows are again of the order of 10 ms^{-1}.

4. CONCLUSION

This paper has outlined the challenge of understanding the complex dynamics of the solar convection zone, and has highlighted some results from two investigations using large-scale numerical simulations. Many previous investigations of solar convection have adopted the DNS approach, and have been faced with the problem of having to introduce large artificial thermal diffusivities and viscosities. The first investigation presented here is of this type, and employs spherical harmonics to expand the prognostic variables. The second investigation presented is of a very different type, employing NFT advection techniques to create an implicitly stable numerical scheme that avoids the use of large amounts of artificial thermal diffusivity and viscosity. Simulations carried out under this philosophy are known as VLES—these results are presented along with results obtained using the same code but adding artificial viscosity and diffusion; this enables comparison with the already-presented DNS results.

All three sets of results (the DNS with spherical harmonic code, the DNS with the NFT code, and the VLES with the NFT code) show similar patterns of vertical velocity in the convection zone, with 'banana-cell' convective rolls and convection velocities of the order of a few hundred meters per second. The DNS and the VLES solutions also show very similar patterns of mean meridional circulation, an aspect of the flow that is important for dynamo wave propagation. The three differ, however, when we come to compare the differential rotation produced—the DNS with the spherical harmonic code gives a somewhat similar pattern to the DNS with the NFT code, but the VLES with the NFT code is rather different. Since the first two are carried out with almost identical equation sets and parameter values, one would expect them to give similar results—the fact that there are differences at all indicates the sensitivity of the solutions to the details of the viscous stresses. On the other hand, the VLES simulation giving such different results is interesting and illustrates particularly well the strong effect of the artificial viscosity and diffusivity used in DNS simulations. Aside from the differences between the three simulations presented, each captures some elements of the observed results that the others do not, so no one could clearly be qualified as the most accurate—comparing the three provides some hints as to the sensitivities of solar convection.

Future work in these investigations will concentrate on better understanding the origin and consequences of the discrepancies between the DNS simulation carried out with the spherical-harmonic code (as described in Section 2), and that carried out with the NFT code (as described in Section 3). In addition, further studies will be carried out to investigate the degree of convergence of the VLES results—were the results from this simulation to change significantly with resolution, it would indicate a poor degree of numerical convergence. If, even in the converged case, the results fail to show good agreement with the observationally determined solar differential rotation, the suggestion would be that some other aspect of the physics of the problem has been incorrectly modeled, whether it is the lack of magnetic fields, insufficient density contrast across the domain, or other factors. There is clearly much scope for further investigation of this fascinating problem.

APPENDIX

This appendix describes the equation sets solved in the two models. We first describe the equations solved in the spherical harmonic code—in this case the prognostic variables are velocity and entropy (in contrast with velocity and potential temperature in the case of the NFT model of Smolarkiewicz). The continuity equation in the anelastic approximation (which applies to both models) is:

$$\nabla \cdot (\rho_0 \mathbf{v}) = 0 \tag{1}$$

where ρ_0 is the reference-state density and $\mathbf{v}$ is the fluid velocity. The momentum equation is

$$\frac{\partial \mathbf{v}}{\partial t} + (\mathbf{v} \cdot \nabla)\mathbf{v} = -\frac{1}{\rho_0} \nabla p' + \frac{\rho'}{\rho_0}\mathbf{g} + 2\mathbf{v} \wedge \mathbf{\Omega} - \frac{1}{\rho_0} \nabla \cdot \mathbf{D} \tag{2}$$

where p' and ρ' are the departures of the pressure and density from the reference state values, $\mathbf{g}$ is the acceleration due to gravity, $\mathbf{\Omega}$ is the rotation vector, and $\mathbf{D}$ is the viscous stress tensor,

given by:

$$D_{ij} = -2\rho_0 v \left[\mathbf{e}_{ij} - \frac{1}{3} (\nabla \cdot \mathbf{v}) \delta_{ij} \right]$$

The entropy equation is given by

$$\rho_0 T_0 \frac{\partial S'}{\partial t} + \rho_0 T_0 (\mathbf{v} \cdot \nabla) S' = \varepsilon + \nabla \cdot (\kappa \rho_0 T_0 \nabla S') + 2v\rho_0 \left[e_{ij} e_{ij} - \frac{1}{3} (\nabla \cdot \mathbf{v})^2 \right] \tag{3}$$

where S' is the fluctuation of entropy away from the reference state value, κ is the thermal diffusivity, and ε is the divergence of the radiative flux. The last term on the right hand side of this equation is the viscous heating term. In all the simulations described in this paper, the following form is used for ε:

$$\varepsilon = \alpha \left(\frac{\zeta_1 e^{-\zeta_1 z}}{1 - e^{-\zeta_1}} - \frac{\zeta_2 e^{-\zeta_2 (1-z)}}{1 - e^{-\zeta_2}} \right) \tag{4}$$

where α is an appropriate constant of proportionality, z is the non-dimensional height within the domain, and ζ_1 and ζ_2 are non-dimensional constants, which take the values 5.5 and 13.0 respectively.

Finally, an equation of state is required to link fluctuations of the entropy to fluctuations of the pressure and density. This is given by the following equation:

$$S' = \frac{3}{2} kT (p'/p_0 - \gamma^{-1} \rho'/\rho_0) \tag{5}$$

where γ is the adiabatic exponent, and k is the Boltzmann constant.

We now proceed to describe the equation set used in the NFT model of Smolarkiewicz. Potential temperature is used instead of entropy, leading to the following momentum and potential temperature equations:

$$\frac{\partial \mathbf{v}}{\partial t} + (\mathbf{v} \cdot \nabla) \mathbf{v} = -\nabla \left(\frac{p'}{\rho_0} \right) + g \frac{\theta'}{\theta_0} + 2\mathbf{v} \wedge \mathbf{\Omega} - \frac{1}{\rho_0} \nabla \cdot (v \rho_0 \nabla \mathbf{v}) \tag{6}$$

$$\frac{\partial \theta'}{\partial t} + (\mathbf{v} \cdot \nabla) \theta' = \frac{\theta_0}{\rho_0 K T_0} \varepsilon - \frac{1}{\rho_0} \nabla \cdot (\kappa \rho_0 \nabla \theta') + 2v\rho_0 \left[e_{ij} e_{ij} - \frac{1}{3} (\nabla \cdot \mathbf{v})^2 \right] \tag{7}$$

where θ' is the fluctuation of potential temperature away from the reference state, and K is the thermal capacity of the fluid. Note the somewhat different form of the viscous stress in the momentum equation. This term is calculated by means of scalar Laplacians on each component, rather than taking the full vector Laplacian—this means that certain parts of the stress (in particular those arriving from the curvature of the coordinate system) are neglected.

ACKNOWLEDGEMENTS

The National Center for Atmospheric Research, NCAR, is operated by the University Corporation for Atmospheric Research under sponsorship of the National Science Foundation. This work has been supported in part by the U.S. Department of Energy "Climate Change Prediction Program" (CCPP) research initiative.

REFERENCES

1. Thompson MJ *et al.* Differential rotation and dynamics of the solar interior. *Science* 1996; **272**:1300–1305.
2. Gough DO. The anelastic approximation for thermal convection. *Journal of the Atmospheric Sciences* 1969; **26**: 448–456.
3. Gilman PA. Nonlinear dynamics of Boussinesq convection in a deep rotating spherical shell. *Geophysical and Astrophysical Fluid Dynamics* 1977; **8**:93–135.
4. Glatzmaier GA. Numerical simulations of stellar convective dynamos. I. The model and method. *Journal of Computational Physics* 1984; **55**:461–484.
5. Elliott JR, Miesch MS, Toomre J. Turbulent solar convection and its coupling with rotation: the effects of Prandtl number and thermal boundary conditions on the resulting differential rotation. *Astrophysical Journal* 2000; **533**:546–556.
6. Miesch MS, Elliott JR, Toomre J, Clune T, Glatzmaier GA. Spherical shell convection with the ASH code. *Astrophysical Journal* 2000; **532**:593–615.
7. Smagorinsky J. General circulation experiments with the primitive equations. *Monthly Weather Review* 1963; **91**:99–152.
8. Margolin LG, Smolarkiewicz PK, Sorbjan Z. Large-eddy simulations of convective boundary layers using nonoscillatory differencing. *Physica D* 1999; **133**:390–397.
9. Smolarkiewicz PK, Margolin LG. MPDATA: A finite-difference solver for geophysical flows. *Journal of Computational Physics* 1998; **140**:459–480.
10. Cattaneo F, Brummell NH, Toomre J, Malagoli A, Hurlburt N. Turbulent Compressible Convection. *Astrophysical Journal* 1991; **370**:282–294.
11. Colella P, Woodward PR. The Piecewise Parabolic Method (PPM) for gas-dynamical simulations. *Journal of Computational Physics* 1984; **54**:174–201.
12. Clune T, Elliott JR, Glatzmaier GA, Miesch MS, Toomre J. Computational aspects of the ASH code. *Parallel Computing* 1999; **25**(4):361–380.
13. Giles PM, Duvall TL, Scherrer PH, Bogart RS. A subsurface flow of material from the Sun's equator to its poles. *Nature* 1997; **390**:52–54.
14. Smolarkiewicz PK, Margolin LG, Wyszogrodzki AA. A class of global nonhydrostatic models. *Journal of the Atmospheric Sciences* 2001; **58**:349–364.

